Available online at www.sciencedirect.com

SciVerse ScienceDirect

Ceramics International 38 (2012) 3673–3681

CERAMICS INTERNATIONAL

www.elsevier.com/locate/ceramint

Improvements on the thermal shock behaviour of MgO–spinel composite refractories by incorporation of zircon–3 mol% Y_2O_3

Cemail Aksel *, Tuba Aksoy

Department of Materials Science and Engineering, Anadolu University, Iki Eylul Campus, Eskisehir 26470, Turkey

Received 20 August 2011; received in revised form 17 December 2011; accepted 4 January 2012
Available online 12 January 2012

Abstract

The effects of incorporations of zircon–3 mol% Y_2O_3 (Y) into MgO–spinel (M–S) compositions to improve mechanical properties and thermal shock behaviour were investigated. Mechanical properties were measured, $R - R_{st}$ parameters were calculated, and thermal shock tests were performed. Microstructural features were examined using SEM and XRD. By adding zircon + Y to M–S: (i) up to ~2 and ~3-fold improvements were achieved in mechanical properties and $R - R_{st}$ parameters, (ii) there were improvements up to ~2-fold in strength data measured after performing thermal shock tests at 1000 °C. Parameters improving mechanical properties and thermal shock behaviour of M–S–(zircon + Y) materials are given as follows: (i) interlinking and arresting or deviation of microcracks when reaching the ZrO_2–Y_2O_3 grains or pores, increases in (ii) K_{Ic}, (iii) critical defect size and (iv) bulk density, (v) formation of forsterite phase, (vi) coexistence of intergranular and transgranular fractures, and (vii) reduction in MgO grain size, leading to longer service life.

Keywords: C. Thermal shock resistance; D. $MgAl_2O_4$; $ZrSiO_4$; Y_2O_3

1. Introduction

Magnesium aluminate spinel ($MgAl_2O_4$) is an important constituent of magnesium oxide (MgO) based refractory materials. The most important factor in MgO–spinel (M–S) refractories' being used prevalently among the other MgO and dolomite originated refractory materials is their much higher resistance to thermal shocks and alkali attacks [1]. In MgO–chrome refractories, concerns on allergy, ulcer and carcinogen effects on skin of the toxic Cr^{6+} ions derived from CrO_3 have led to the need for use of no-chromium containing alternative MgO–spinel refractories [2]. MgO–spinel refractories have service lives ~1.5–2 times longer than MgO–chrome refractories [3]. MgO–spinel bricks are preferred in the cooling and transition zones where thermal stresses occur due to high temperature difference and therefore severe thermal shocks taking place during cooling and heating in cement rotary kilns [4]. In addition, their use in the sintering zone that requires adequate strength at high temperature affords economic benefits [4]. Furthermore, the side walls and bottom of steel teeming ladles and the checker work of glass tank furnace regenerators are also other major application areas of spinel refractories [4,5]. The stoichiometric type is similarly used in cement kiln linings, as well as an alumina based castable in ladles, which can also have high resistance to corrosion, erosion and abrasion caused by calcium–aluminium–silicate containing compounds [3]. MgO–spinel refractories are preferred as they show high thermal shock resistance, high resistance against basic slag and alkali attacks, including molten metal abrasions [1].

It is reported [1,4–9] that the addition of spinel to MgO markedly improves hot modulus of rupture, the retained strength after thermal shock, refractoriness under load, and also incorporation of additives such as Y_2O_3 into MgO–spinel significantly develops densification and hot strength characteristics of MgO–spinel composite refractory materials. While service life of MgO–spinel refractories is prolonged especially in connection with the rise in work of fracture energy when spinel particles are added to MgO, a reduction occurs in other mechanical properties [10–12]. This study has been conducted for improving the mechanical and thermal shock performances of materials further and prolonging service life further by

* Corresponding author. Tel.: +90 222 3350580x6362; fax: +90 222 3239501.
E-mail address: caksel@anadolu.edu.tr (C. Aksel).

0272-8842/$36.00
doi:10.1016/j.ceramint.2012.01.009

obtaining high thermo-mechanical properties due to the increase especially in resistance to fracture by additions of zircon and Y_2O_3 in different proportions to various MgO–spinel compositions. The relationships between the mechanisms causing improvements in the mechanical–thermal shock behaviours of composite refractories and microstructural changes and parameters affecting these were examined and explained citing reasons.

2. Materials and methods

Recipes were prepared by incorporating 5, 10, 20 and 30% zircon ($ZrSiO_4$) by weight and 3 mol% Y_2O_3 (Y) correlated with ZrO_2 content in zircon into MgO (M) based compositions containing 5, 10, 20 and 30% $MgAl_2O_4$ spinel (S) by weight (Table 1). The amounts of 3 mol% Y_2O_3 equivalent to ZrO_2 proportion in zircon were calculated for each composition, where those quantities of Y_2O_3 were subsequently converted to weight percentages, and given in Table 1. Batches using MgO (0–1 mm, 95.7% purity, Konya Selcuklu Krom Magnezit Tugla Sanayi A.S., Turkey), spinel (0–1 mm, 64.1% Al_2O_3 and 34.1% MgO, Konya Selcuklu Krom Magnezit Tugla Sanayi A.S., Turkey), zircon (~13 μm, 64.0% ZrO_2 and 32.5% SiO_2, Colorobbia, Turkey) and Y_2O_3 (~4 μm, 99.9% purity, Colorobbia, Turkey) were prepared. After incorporating 1.5% $MgSO_4$ and 1% totanin by weight as binder solutions into each batch, they were mixed in a mixer (IKA, Labortechnik) for ~5 min with a speed of 7000 rpm. Those batches were shaped into samples of ~8 mm × 8 mm × 60 mm under a pressure of ~100 MPa. The samples were sintered for 2 h in a kiln (Nabertherm HT16/18) at 1600 °C using heating and cooling rates of 5 °C/min. Bulk density (ρ) and apparent porosity values of 3 specimens from each composition were measured using the standard water immersion method and average values were taken [13]. After samples were ground using 800 and 1200 grade SiC papers until smooth surfaces were obtained based on the standard sample preparation rules [11,14], the samples were dried at ~110 °C in an oven and mechanical tests were carried out. The mechanical tests performed using a load cell of 2 kN moving at a velocity of 0.5 mm/min with a support roller span (L) of 40 mm were applied to minimum 5–6 samples and average values were taken. Under standard tests; values of strength [14] (σ), modulus of elasticity [15] $\{E = L^3m/(4WD^3)\}$, fracture toughness [16–19] $\{K_{Ic} = (3/2)(PLc^{1/2}Y)/(WD^2)\}$, fracture surface energy, γ_S [20], $\{K_{Ic} = (2E\gamma_S)^{1/2}\}$ and work of fracture energy [21] $\{\gamma_{WOF} = U/[2W(D - c)]\}$ were determined by the 3-point bending method in Instron 5581. The parameters used in the equations given above are as follows [14–21]: m is slope of the tangent of the initial straight-line portion of the load–deflection curve, W is the specimen width, D is the specimen thickness, P is the load at failure, c is the notch depth, and Y is a dimensionless constant depending on the geometry of loading and crack configuration, where $\{Y = A_0 + A_1(c/D) + A_2(c/D)^2 + A_3(c/D)^3 + A_4(c/D)^4\}$, for L/D ~8, $A_0 = 1.96$, $A_1 = -2.75$, $A_2 = 13.66$, $A_3 = -23.98$, $A_4 = 25.22$ [16,19]. Work of fracture is usually interpreted as the work done in propagating a crack to break a notched specimen, divided by twice the fracture surface areas (since two new faces are created). γ_{WOF} is the amount of energy required to propagate a crack completely through a specimen, which is calculated by determining the area remaining under the load–deflection curve (U) [21]. The magnitude of critical defect size (C) value was calculated using Griffith equation [20,22], where combining K_{Ic} data with those of strength allowed an estimate to be made of the critical defect size [10,11]. E values were calculated using the steepest slope in the initial linear portion of the stress–strain curve, where the correction for machine stiffness was also considered. K_{Ic}, γ_S and γ_{WOF} measurements were performed using Single Edge Notched Beam (SENB) method [16–21] at a depth of ~25% of thickness of the material using a 700 μm thick diamond disk on specimens. Notch depth was measured using an Olympus BX60M brand optical microscope. X-ray diffraction (XRD) analysis was performed using Rigaku RINT2000 equipment. The polishing of specimens for scanning electron microscope (SEM) examination was carried out for ~3.5 min using a 1 μm diamond spray at the final stage and samples were thermally etched at 1450 °C for 10 min to reveal grain boundaries in the microstructure. SEM studies were carried out on Zeiss Evo 50 and JSM-5910LV devices analyzing microstructures and fracture surfaces of materials. The mean MgO grain size was calculated by a standard line mean intercept method [23], using 3 SEM pictures taken on the polished and thermally etched surface of the specimen. Hasselman parameters, which determine the fracture resistance of materials due to thermal stress/shock and used in estimation of maximum thermal

Table 1
Compositions prepared for mechanical and thermal shock tests in which weights of MgO (0–1 mm), spinel (0–1 mm), $ZrSiO_4$ (~13 μm) and 3 mol% Y_2O_3 (~4 μm) correlated with ZrO_2 content in $ZrSiO_4$ were used.

Compositions	MgO (M) (%)	Spinel (S) (%)	$ZrSiO_4$ (zircon) (%)	Y_2O_3[a] (Y) (%)
M	100.00	–	–	–
M–5%S	95.00	5	–	–
M–10%S	90.00	10	–	–
M–20%S	80.00	20	–	–
M–30%S	70.00	30	–	–
M–5%S–5%(zircon + Y)	89.83	5	5	0.17
M–5%S–10%(zircon + Y)	84.66	5	10	0.34
M–5%S–20%(zircon + Y)	74.31	5	20	0.69
M–5%S–30%(zircon + Y)	63.97	5	30	1.03
M–10%S–5%(zircon + Y)	84.83	10	5	0.17
M–10%S–10%(zircon + Y)	79.66	10	10	0.34
M–10%S–20%(zircon + Y)	69.31	10	20	0.69
M–10%S–30%(zircon + Y)	58.97	10	30	1.03
M–20%S–5%(zircon + Y)	74.83	20	5	0.17
M–20%S–10%(zircon + Y)	69.66	20	10	0.34
M–20%S–20%(zircon + Y)	59.31	20	20	0.69
M–20%S–30%(zircon + Y)	48.97	20	30	1.03
M–30%S–5%(zircon + Y)	64.83	30	5	0.17
M–30%S–10%(zircon + Y)	59.66	30	10	0.34
M–30%S–20%(zircon + Y)	49.31	30	20	0.69
M–30%S–30%(zircon + Y)	38.97	30	30	1.03

[a] The amounts of 3 mol% Y_2O_3 equivalent to ZrO_2 proportion in zircon were calculated for each composition and afterwards those quantities of Y_2O_3 (Y) were converted to weight percentages.

Table 2
Strength (σ), modulus of elasticity (E), fracture surface energy (γ_S) and critical defect size (C) values of MgO, M–S and M–S–(zircon + Y) composite refractories containing varied amounts of additives.

Compositions	σ (MPa)	E (GPa)	γ_S (J/m^2)	C (μm)
M	48.5 ± 5.5	35.1 ± 2.4	32.8 ± 3.7	310.5
M–5%S	21.9 ± 4.2	20.4 ± 4.9	22.9 ± 3.3	617.1
M–10%S	14.8 ± 1.0	14.7 ± 1.3	14.5 ± 2.3	611.8
M–20%S	11.4 ± 0.4	8.2 ± 0.9	17.4 ± 2.0	698.9
M–30%S	11.3 ± 0.5	7.9 ± 0.9	16.4 ± 2.6	638.4
M–5%S–5%(zircon + Y)	15.6 ± 3.1	15.9 ± 2.2	27.0 ± 6.5	1109.8
M–5%S–10%(zircon + Y)	23.2 ± 3.1	19.8 ± 2.0	21.2 ± 3.8	491.5
M–5%S–20%(zircon + Y)	20.4 ± 3.7	18.0 ± 2.6	25.1 ± 6.8	678.2
M–5%S–30%(zircon + Y)	23.5 ± 3.8	18.4 ± 2.6	28.6 ± 8.5	593.3
M–10%S–5%(zircon + Y)	11.4 ± 0.3	11.4 ± 1.5	14.3 ± 2.2	793.7
M–10%S–10%(zircon + Y)	15.0 ± 2.1	12.1 ± 0.7	21.4 ± 3.5	729.3
M–10%S–20%(zircon + Y)	17.0 ± 2.0	14.9 ± 1.7	18.8 ± 5.1	603.4
M–10%S–30%(zircon + Y)	21.6 ± 1.8	18.3 ± 1.4	26.3 ± 4.2	653.3
M–20%S–5%(zircon + Y)	12.3 ± 0.4	9.2 ± 1.0	16.9 ± 3.0	656.1
M–20%S–10%(zircon + Y)	14.9 ± 1.0	10.6 ± 0.9	15.4 ± 3.6	463.8
M–20%S–20%(zircon + Y)	17.2 ± 2.3	11.9 ± 1.9	18.0 ± 5.3	453.0
M–20%S–30%(zircon + Y)	19.9 ± 2.9	15.4 ± 0.7	22.9 ± 4.1	569.0
M–30%S–5%(zircon + Y)	15.1 ± 1.0	11.6 ± 1.2	17.6 ± 3.4	565.2
M–30%S–10%(zircon + Y)	16.9 ± 1.1	12.9 ± 1.0	20.9 ± 4.8	593.1
M–30%S–20%(zircon + Y)	21.3 ± 4.0	15.2 ± 2.9	39.0 ± 7.7	829.9
M–30%S–30%(zircon + Y)	32.5 ± 1.9	21.4 ± 0.2	33.2 ± 3.1	428.8

resistance, were calculated by following formulas [24]: $\{R = [\sigma(1-\nu)]/(E\alpha)\}$ and $\{R_{st} = [\gamma_S/(\alpha^2 E)]^{1/2}\}$, where ν is the mean value of Poisson's ratio and α is the mean thermal expansion coefficient of the composite refractory. Thermal shock tests were performed by sudden cooling in water from 500 and 1000 °C to 25 °C room temperature with strength values determined in connection with thermal shock temperatures.

3. Results and discussion

Mechanical tests data of composite refractories produced by incorporating varied amounts of $ZrSiO_4$ + 3 mol% Y_2O_3 (zircon + Y) into MgO–spinel (M–S) materials containing varied ratios of spinel ($MgAl_2O_4$) are given below. The additives used in figures and tables show: (i) $MgAl_2O_4$ for M–S, and (ii) $ZrSiO_4 + Y_2O_3$ for M–S–(zircon + Y) materials.

As seen in Table 2, it was observed that as the amount of additives (i.e. both zircon and Y_2O_3) was increased, there was generally a marked enhancement in the strength (σ) and modulus of elasticity (E) values of M–S–(zircon + Y) composite refractories compared to M–S materials. This development was significant especially with incorporation of ≥10% zircon + Y additives into M–S for σ and E values, where both of them reached to maximum level on M–30%S–30%(zircon + Y) composition. A 2.9-fold increase in σ data and 2.7-fold rise in E values were achieved with the addition of 30%(zircon + Y) to M–30%S (Table 2).

The fracture toughness (K_{Ic}) data of composite refractories obtained by adding varied ratios of ≥10%(zircon + Y) to M–S compositions were in general higher than those of M–S materials (Fig. 1). It was observed that K_{Ic} values of all composites containing 30% zircon + Y additives were close to each other. For instance; in K_{Ic} values obtained as a result of incorporation of 20% and 30% zircon + Y into M–30%S, improvements of 2.1-fold and 2.2-fold were attained respectively in comparison with M–30%S (Fig. 1). As shown in Table 1, fracture surface energy (γ_S) values of M–S–(zircon + Y) composite refractories were generally higher than the γ_S values of M–S materials, especially when ≥10%(zircon + Y) is incorporated into M–S compositions. In the γ_S values obtained by incorporating 20% and 30% zircon + Y into M–30%S–(zircon + Y) composition, 2.4-fold and 2.0-fold improvements were observed respectively compared to M–30%S material, where γ_S values were consistent with K_{Ic} data (Table 2 and Fig. 1).

When the critical defect size (C) values were examined in Table 2, a marked rise was observed in the C values of all M–S and M–S–(zircon + Y) compositions into which additives were incorporated, compared to the additive free MgO. In general, the majority of M–S–(zircon + Y) compositions had lower

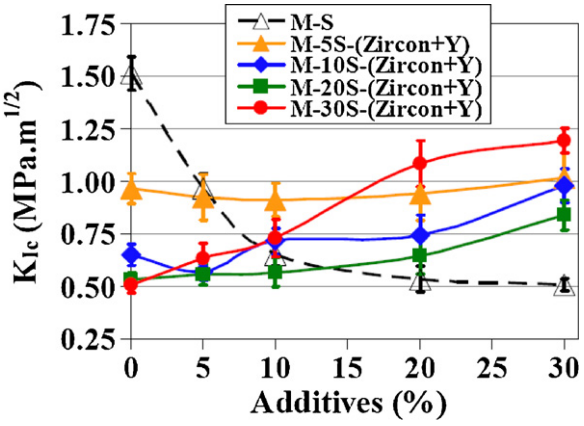

Fig. 1. Fracture toughness (K_{Ic}) as a function of additives {additives: (i) $MgAl_2O_4$ for M–S, and (ii) $ZrSiO_4 + Y_2O_3$ for M–S–(zircon + Y)}.

C values than those of M–S composites; however, some parts of them were found to be equivalent to or predominantly much higher than the critical defect size of M–S materials. This increase in *C* data was associated with the improvement in K_{Ic} values, showing a high resistance to fracture.

Work of fracture energy (γ_{WOF}) values were calculated for different compositions selected as follows: (i) MgO = 27.4 ± 3.1 J/m^2, (ii) M–5%S = 63.9 ± 15.2 J/m^2, (iii) M–5%S–5%(zircon + Y) = 65.2 ± 13.6 J/m^2, (iv) M–30%S = 67.6 ± 6.7 J/m^2, (v) M–30%S–10%(zircon + Y) = 66.3 ± 4.6 J/m^2 and (vi) M–30%S–30%(zircon + Y) = 60.6 ± 8.9 J/m^2. The γ_{WOF} values of M–S and M–S–(zircon + Y) composite refractories were quite close to each other. It was determined that the incorporations of varied amounts of both (i) spinel into M–S and (ii) zircon + Y into M–S–(zircon + Y) compositions improved the γ_{WOF} data reaching up to ~2.5-fold ratios in comparison with additive free MgO.

Fig. 2 illustrates that bulk density (ρ) values increased markedly with the increasing quantity of zircon + Y additives. The mean bulk density values measured for M and M–S composite refractories were ~2.8 g/cm^3, rising up to ~3.3 g/cm^3 with increased amounts of added zircon + Y. In M–S–(zircon + Y) compositions; the replacement of heavier constituents such as zircon (ρ_{Zircon}: 4.56 g/cm^3) and Y_2O_3 ($\rho_{Y_2O_3}$: 5.046 g/cm^3), which had higher densities [25,26] in comparison with M–S (ρ_{M-S}: 3.58 g/cm^3), caused an enhancement in bulk density values leading to a decrease in apparent porosity data. In addition, the apparent porosity data was measured to be as ~21% in M and M–S materials, showing a downward trend reaching ~12% with the rise in the amount of zircon + Y incorporated into M–S compositions.

As microstructure and the distribution of elements were examined for M–30%S–30%(zircon + Y) composite refractory, which was chosen as an exemplar sample displaying marked improvements on mechanical properties, it was observed that MgO and SiO_2 distributions were generally located in the similar regions, indicating the formation of forsterite (Mg_2SiO_4) phase (Fig. 3). X-ray diffraction (XRD) analysis results for M–30%S–30%(zircon + Y) composition showed that forsterite ($2MgO.SiO_2$) and cubic zirconia phases were

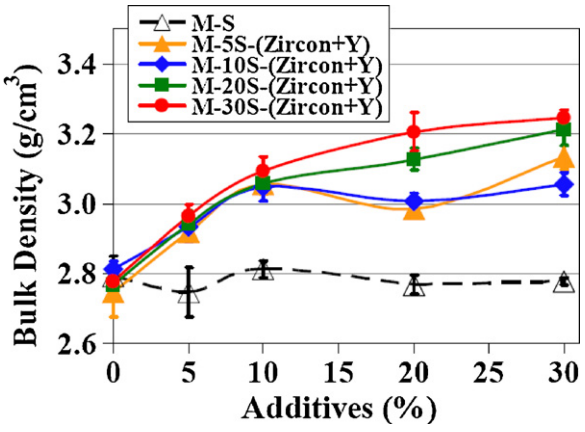

Fig. 2. Bulk density (ρ) as a function of additives {additives: (i) $MgAl_2O_4$ for M–S, and (ii) $ZrSiO_4 + Y_2O_3$ for M–S–(zircon + Y)}.

identified besides MgO and spinel phases (Fig. 4). A stronger bond is formed between the additives and the grains of main constituent as a consequence of the formation of forsterite phase due to the reaction between SiO_2, which is released after dissociation of zircon as ZrO_2 and SiO_2 during sintering, and the main phase MgO. It was determined that sintering was more effective with the formation of the new phase. This is also consistent with the enhancement in bulk density values and the drop in the amount of apparent porosity data occurring as a result of the increase in the quantity of zircon + Y added to M–S compositions.

Microstructural observations in Figs. 3 and 5 demonstrate that the white coloured ZrO_2 grains, which were released after the dissociation of zircon during sintering, were found in the same regions with white coloured Y_2O_3 particles, where they were located mainly at the surrounding of dark gray coloured MgO grains. After sintering M–S–(zircon + Y) containing materials, large tensile stresses occurred around the additives during cooling as a result of the significant difference between the thermal expansion coefficients (α) [25–27] of MgO, spinel, zircon and Y_2O_3 ($\alpha_{MgO} = 13.6 \times 10^{-6}\,^{\circ}C^{-1}$, $\alpha_{Spinel} = 8.4 \times 10^{-6}\,^{\circ}C^{-1}$, $\alpha_{Zircon} = 4.6 \times 10^{-6}\,^{\circ}C^{-1}$, $\alpha_{Y_2O_3} = 60.3 \times 10^{-6}\,^{\circ}C^{-1}$) and such stresses resulted in formation of interlinked microcracks [10–12,28]. It was observed that these microcracks were interlinked to each other and arrested or deviated by propagating for a short distance when reaching the ZrO_2 grains located together with Y_2O_3 or the pores (Figs. 3 and 5). In addition, the mean MgO grain size was calculated for different compositions selected as follows: (i) additive free MgO = 67.2 μm, (ii) M–30%S = 31.2 μm and (iii) M–30%S–30%(zircon + Y) = 23.8 μm. There was a marked reduction in MgO grain size with an enhancement in the quantity of all additives (i.e. spinel and zircon + Y) in comparison with additive free MgO, where the decreases in mean MgO grain size of MgO material by adding additives were determined to be ~2.2-fold for M–30%S and ~2.8-fold for M–30%S–30%(zircon + Y) compositions.

The fracture surface images of the composite refractory materials having compositions of M–30%S and M–30%S–30%(zircon + Y) are given in Fig. 6. It is known from the previous research that there are mainly transgranular cracks on the fracture surface of MgO [10–12,28]. However, when the spinel particles were added to MgO, fracture type turned predominantly into intergranular cracks in M–S materials (Fig. 6a) [10–12,28]. As zircon + Y were added to M–S on the other hand, it was observed that the intergranular and transgranular types of cracks occurred concurrently (Fig. 6b).

Fig. 7 illustrates schematic diagrams of load–deflection curves of additive free MgO and M–30%S–30%(zircon + Y) composite refractory materials. For additive free MgO, there were predominantly transgranular cracks and thus catastrophic failure occurred during fracture (Fig. 7a). However, the fracture path of M–S–(zircon + Y) materials showed a stable behaviour (Fig. 7b). This is due to the coexistence of both intergranular and transgranular cracks on the fracture surface (Fig. 6b), where these types of cracks were observed to propagate around the smaller grains. Therefore, it appears that higher values of

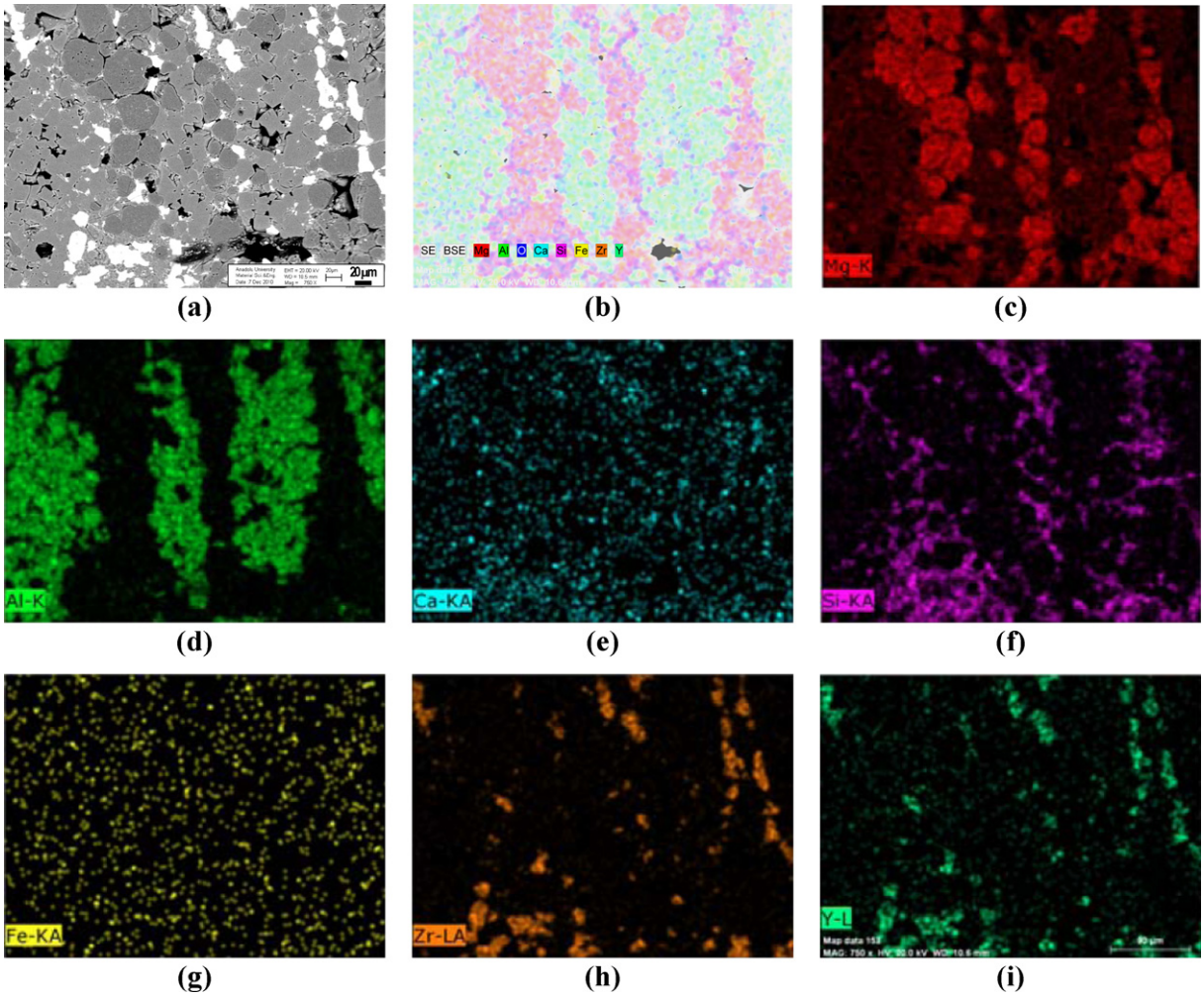

Fig. 3. Microstructural image [(a) and (b)] and distribution of elements [(c) Mg, (d) Al, (e) Ca, (f) Si, (g) Fe, (h) Zr and (i) Y] of the composite refractory material having M–30%S–30%(zircon + Y) composition.

mechanical properties (i.e. especially in K_{Ic}, γ_S and γ_{WOF} values) are also associated with the coexisting of both intergranular and transgranular types of cracks with increasing quantities of zircon + Y in M–S compositions. The alteration in the fracture path of M–S–(Zircon + Y) composite refractories resulted in an enhancement in the areas under the load–displacement curve, which indicated significant microcrack extension and interlinking with the higher K_{Ic}, γ_S and γ_{WOF} values, requiring more energy for the fracture process and thus those materials showed a stable crack growth behaviour.

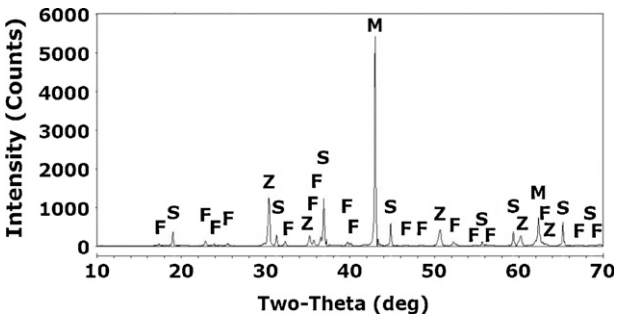

Fig. 4. XRD graph of a composite refractory having M–30%S–30%(zircon + Y) composition (M: MgO, S: $MgAl_2O_4$, F: Mg_2SiO_4 and Z: ZrO_2).

Significant parameters in general enhancing the mechanical properties and hence leading to an improvement in thermal shock behaviour of M–S–(zircon + Y) materials were found to be; occurrence of the above-listed structural changes: (a) in the microstructure and (b) on the fracture surfaces, and with the addition of zircon + Y to M–S, rises in (c) K_{Ic}, (d) C and (e) bulk density, (f) formation of forsterite phase, and (g) decrease in the grain size of MgO.

R thermal stress parameter [24] values, which represent the minimum temperature difference required for the initiation of fracture, showing the resistance against the initiation of the crack in the material are given in Fig. 8. M–≥20%S materials to which varied ratios of zircon + Y were added displayed a greater crack initiation resistance with higher R values compared to M–S compositions. It was observed that spinel content (e.g. especially at ≥20%S), together with the increasing amount of zircon + Y, was also instrumental in the enhancement of R data. In M–S–(zircon + Y) materials; when SiO_2 reacts with MgO the forsterite (Mg_2SiO_4) phase forms during sintering, where the bonding between MgO grains becomes

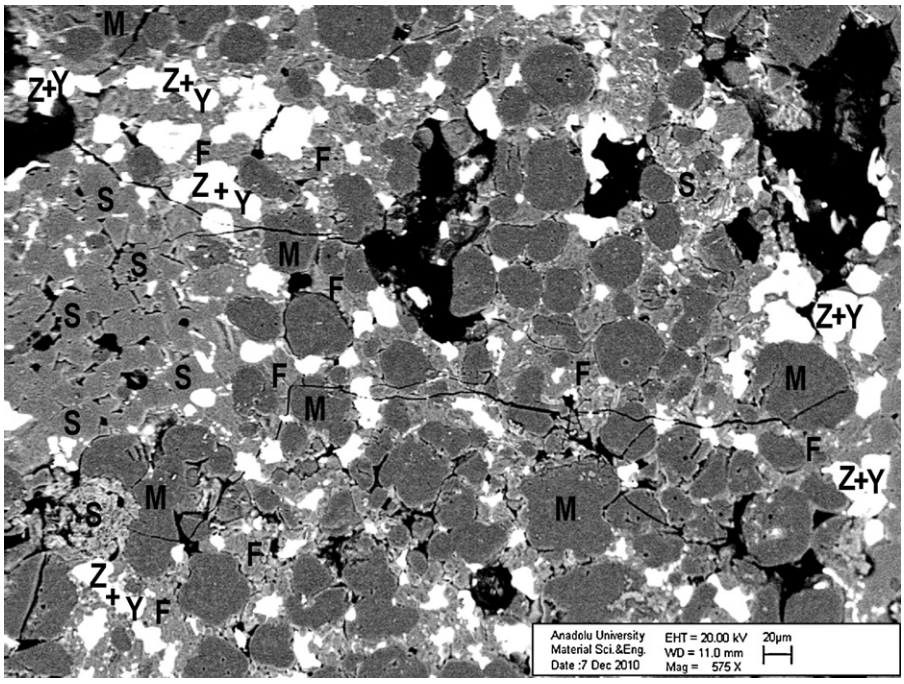

Fig. 5. Microstructural image of a material with composition of M–30%S–30%(zircon + Y) {dark gray: MgO (M), light gray: $MgAl_2O_4$ (S) and Mg_2SiO_4 (F), and white zones: ZrO_2 (Z) and Y_2O_3 (Y)}.

stronger and in association with it, the crack initiation resistance enhances. In general; R values of M–S–(zircon + Y) compositions were higher than those of M–S materials, and reached to a maximum level in M–30%S–30%(zircon + Y) composition. When M–30%S–30%(zircon + Y) material was compared to M–S compositions having minimum and maximum R values, which are (i) M–10%S and (ii) M–30%S, it was determined that higher resistance could be achieved against initiation of the crack at ratios reaching (i) 1.9-fold and (ii) 1.2-fold, respectively.

The R_{st} parameter represents the maximum temperature difference allowed required for propagation of long cracks under severe thermal stress conditions and is used in estimating the further weakening of the composite refractory and crack stability with the increase in the severity of thermal shock [24]. Fig. 9 shows that the highest R_{st} parameter values were firstly attained in M–30%S–20%(zircon + Y) and afterwards in M–30%S–30%(zircon + Y) compositions in comparison with M and M–S materials. As M–30%S–20%(zircon + Y) material was compared to (i) M–10%S and (ii) M–30%S, where these M–S compositions had minimum and maximum R_{st} values, it was determined that higher resistance to thermal shocks could be achieved in ratios reaching (i) 2.0-fold and ii) 1.2-fold, respectively. In addition, it was also found that the R_{st} value of M–30%S–30%(zircon + Y) material was slightly higher than that of M–30%S, which had maximum R_{st} data in M–S compositions, and there was a marked improvement reaching 1.6-fold in the R_{st} data of M–30%S–30%(zircon + Y) compared

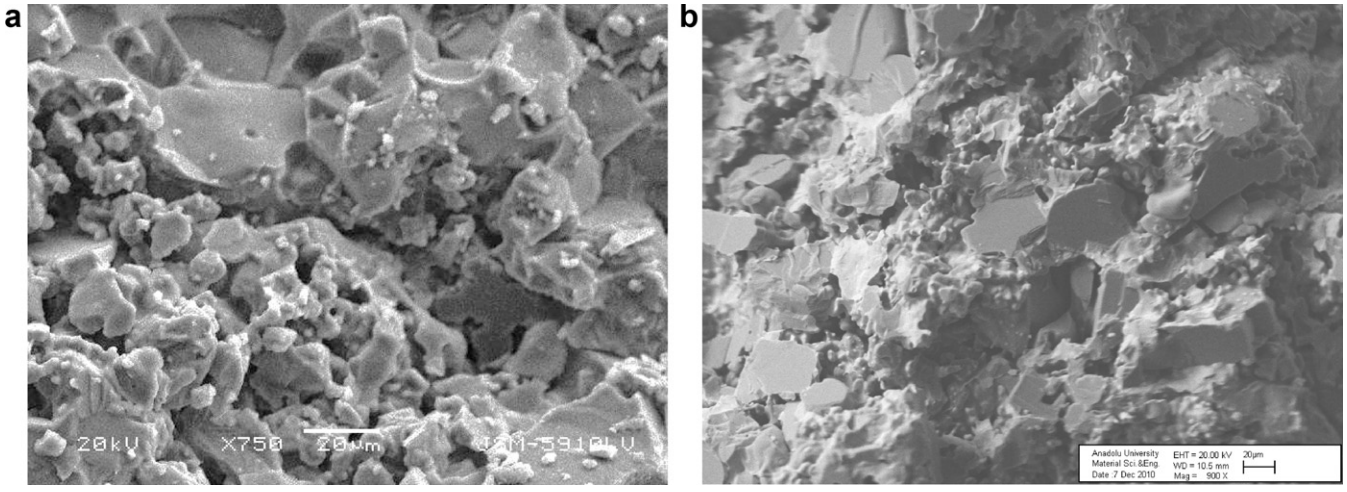

Fig. 6. Fracture surface images of materials with compositions of (a) M–30%S and (b) M–30%S–30%(zircon + Y).

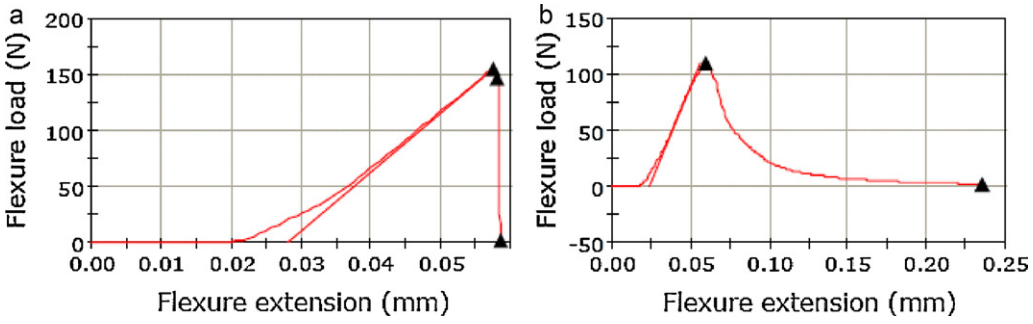

Fig. 7. Load–deflection curves for centred notched, 3-point bending specimens: (a) MgO (catastrophic), and (b) M–30%S–30%(zircon + Y) (stable).

to M–10%S having minimum R_{st} value among the M–S composite refractories.

It was determined that R and R_{st} parameters were generally in accord with each other, and the incorporations of zircon–Y_2O_3 into M–S compositions improved both crack initiation resistance and crack stability preventing the further weakening of composite refractory materials under severe thermal conditions. The R and R_{st} parameter values showed that M–30%S–30%(zircon + Y) and M–30%S–20%(zircon + Y) composite refractories displayed higher thermal stress resistance and thermal shock damage resistance compared to M and M–S materials that also illustrate consistency with the determined mechanical properties.

Strength (σ) values measured after thermal shock tests, which were performed for M, M–S and M–S–(zircon + Y) materials, were determined as a function of thermal shock temperature (Fig. 10). The σ values displayed a periodical decrease with increasing thermal shock temperature. There was also a sharp drop in the σ values of MgO with increasing thermal shock temperatures, which were measured to be as 48.5 ± 5.5 MPa at 25 °C, 10.8 ± 0.7 MPa at 500 °C and 6.1 ± 0.4 MPa at 1000 °C. At 500 °C and 1000 °C thermal shock temperatures, M–S–(zircon + Y) composite refractories, when compared to M and M–S materials, have σ data that are close to each other in some compositions; however, have significantly higher σ values in certain other compositions. In general, thermal shock test results indicate a similar trend with the data of R and R_{st} parameters and verify the R and R_{st} values.

Therefore, the R and R_{st} thermal stress/shock parameters were determined to be reliable indicators, which might be used in determining the thermal behaviour of composite refractories. In addition, the increases in K_{Ic} indicating a high resistance to fracture and C, which led to development of crack propagation resistance, were also found to be basic factors in the improvement of thermal shock resistance, and the results obtained were consistent with the thermal shock data.

The quantity and lengths of pre-formed microcracks occurred due to the α differences of constituents and newly formed microcracks after application of thermal shock were smaller and limited in M–S–(zircon + Y) materials. The microstructural variations and features stated above were associated with the improvement occurring in the mechanical and thermal shock behaviours of zircon + Y added M–S materials.

The material with the highest strength value, undergoing thermal shock tests at 500 °C and 1000 °C, produced by adding varied proportions of zircon + Y to M–S composite refractories was found to be M–30%S–30%(zircon + Y). For example, in the thermal shock tests performed at 1000 °C, M–30%S–30%(zircon + Y) composition has respectively (i) 2.0-fold, (ii) 1.9-fold and (ii) 1.7-fold higher strength values when compared to (i) MgO, (ii) M–10%S and (iii) M–30%S, in which M–10%S has demonstrated the lowest thermal shock resistance among M–S materials. This improvement is consistent with the low loss of strength at high temperatures, high thermal shock damage resistance and consequently longer service lives of M–S–(zircon + Y) composite refractories for industrial uses.

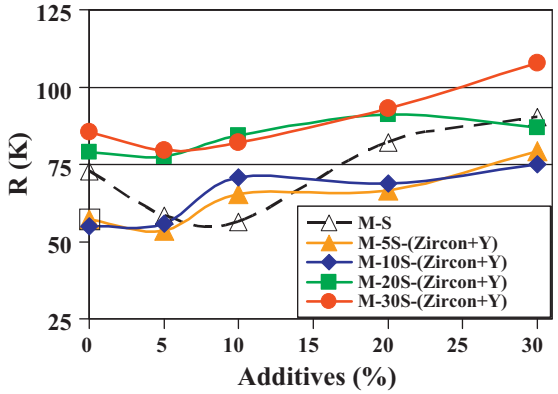

Fig. 8. R parameter as a function of additives {additives: (i) $MgAl_2O_4$ for M–S, and (ii) $ZrSiO_4 + Y_2O_3$ for M–S–(zircon + Y)}.

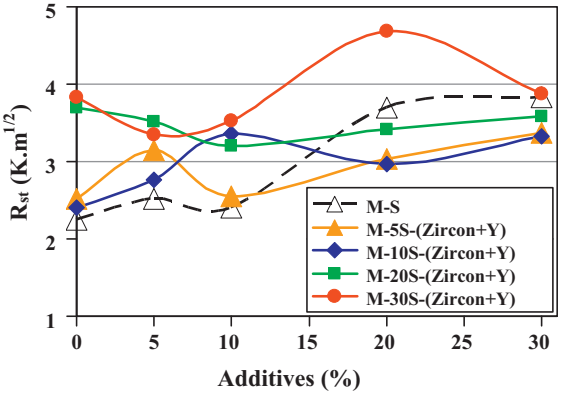

Fig. 9. R_{st} parameter as a function of additives {additives: (i) $MgAl_2O_4$ for M–S, and (ii) $ZrSiO_4 + Y_2O_3$ for M–S–(zircon + Y)}.

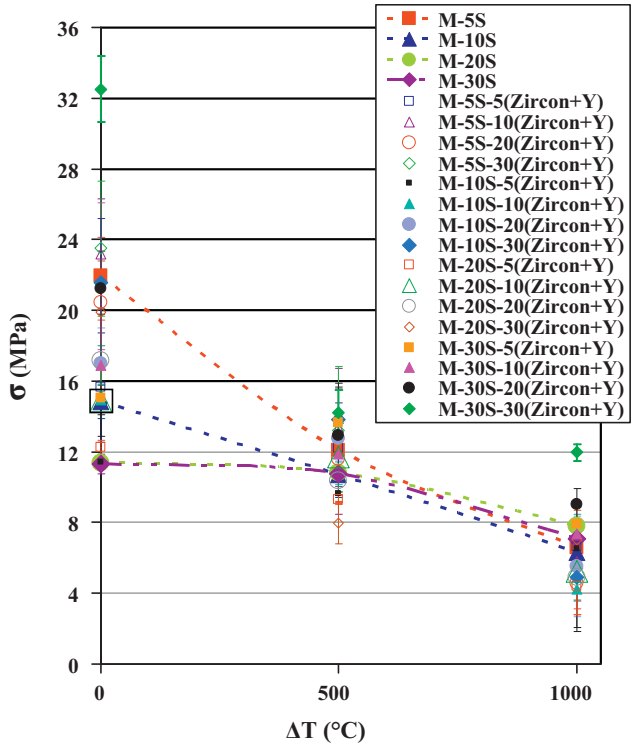

Fig. 10. Strength (σ) values of M–S and M–S–(zircon + Y) composite refractories containing varied amounts of additives as a function of thermal shock temperatures {additives: (i) $MgAl_2O_4$ for M–S, and (ii) $ZrSiO_4 + Y_2O_3$ for M–S–(zircon + Y)}.

4. Conclusions

With the addition of 30%(zircon + Y) to M–30%S, improvements of up to ~2 and ~3-fold ratios were achieved in mechanical properties. The R and R_{st} parameters showed that M–30%S–30%(zircon + Y) materials had ratios reaching respectively up to ~1.9 and ~1.6-fold higher thermal stress and shock resistance in comparison with M–S composite refractories. In M–S–(zircon + Y) materials; when SiO_2, which is released due to decomposition of zircon as ZrO_2 and SiO_2, reacts with MgO, the bonding between MgO grains becomes stronger as a result of the formation of the forsterite (Mg_2SiO_4) phase, and consequently the crack initiation resistance is enhanced. In addition; the rises in K_{Ic} and C, which led to development of crack propagation resistance, were also found to be effective factors to improve the thermal shock resistance of the composite refractory materials. It was determined based on the thermal shock tests performed at 1000 °C that M–30%S–30%(zircon + Y) composition had (i) 2.0-fold, (ii) 1.9-fold and (iii) 1.7-fold higher strength values in comparison respectively with (i) MgO, (ii) M–10%S and (iii) M–30%S materials, where M–10%S displayed the lowest thermal shock resistance among M–S composite refractories. Thermal shock results confirmed the R and R_{st} values, and thus R and R_{st} parameters were found to be reliable indicators for determining the thermal behaviour of composite refractory materials.

The basic parameters improving mechanical properties and thermal shock behaviour of M–S–(zircon + Y) composite refractories were determined as follows: (i) interlinking and arresting or deviation of microcracks when reaching the ZrO_2–Y_2O_3 grains or pores, rises in (ii) fracture toughness and (iii) critical defect size, (iv) increase in bulk density (e.g. decrease in apparent porosity), (v) formation of forsterite phase, (vi) coexistence of intergranular and transgranular cracks, and (vii) decrease in MgO grain size, leading to low loss of strength, high thermal shock damage resistance and longer service life for industrial applications.

Acknowledgements

This study was partly supported by Anadolu University and in part TUBITAK under project no: 106M394 with partial support provided also by Konya Selcuklu Krom Magnezit Tugla Sanayi A.S. We would like to express our gratitude to A. Ozkaymak, R. Ozbasi, O. Bezirci, M. Ilhan and all agency employees and personnel involved in this project for their support. We also thank the agencies and plant authorities for the supplied equipments and raw materials.

References

[1] G.R. Eusner, D.H. Hubble, Technology of spinel bonded periclase brick, J. Am. Ceram. Soc. 43 (1960) 292–296.
[2] D.J. Bray, Toxicity of chromium compounds formed in refractories, Bull. Am. Ceram. Soc. 64 (1985) 1012–1016.
[3] K. Tokunaga, H. Kozuka, T. Honda, F. Tanemura, Further improvements in high temperature strength, coating adherence, and corrosion resistance of magnesia–spinel bricks for rotary cement kiln, in: Proc UNITECR'91 Congress, Aachen, Germany, (1991), pp. 431–435.
[4] R.D. Maschio, B. Fabbri, C. Fiori, Industrial applications of refractories containing magnesium aluminate spinel, Ind. Ceram. 8 (1988) 121–126.
[5] A. Ghosh, R. Sarkar, B. Mukherjee, S.K. Das, Effect of spinel content on the properties of magnesia–spinel composite refractory, J. Eur. Ceram. Soc. 24 (2004) 2079–2085.
[6] P. Bartha, Magnesia spinel bricks–properties, production and use, in: X. Zhong, et al. (Eds.), Proc. Int. Symp. Refractories, Refractory Raw Materials and High Performance Refractory Products, Pergamon, Hangzhou, 1989, pp. 661–674.
[7] C. Aksel, B. Rand, F.L. Riley, P.D. Warren, Thermal shock behaviour of magnesia–spinel composites, J. Eur. Ceram. Soc. 24 (2004) 2839–2845.
[8] R. Sarkar, S.K. Das, G. Banerjee, Effect of additives on the densification of reaction sintered and presynthesised spinels, Ceram. Int. 29 (2003) 55–59.
[9] R. Sarkar, H.S. Tripathi, A. Ghosh, Reaction sintering of different spinel compositions in the presence of Y_2O_3, Mater. Lett. 58 (2004) 2186–2191.
[10] C. Aksel, F.L. Riley, Magnesia-spinel ($MgAl_2O_4$) refractory ceramic composites, in: I.M. Low (Ed.), Ceramic Matrix Composites: Microstructure, Properties and Applications, Woodhead Publishing Limited and CRC Press LLC, USA, 2006, pp. 359–399.
[11] C. Aksel, B. Rand, F.L. Riley, P.D. Warren, Mechanical properties of magnesia–spinel composites, J. Eur. Ceram. Soc. 22 (2002) 745–754.
[12] C. Aksel, P.D. Warren, Work of fracture and fracture surface energy of magnesia–spinel composites, Compos. Sci. Technol. 63 (2003) 1433–1440.
[13] BS 7134, Methods for determination of density and porosity, in: British Standard Testing of Engineering Ceramics, Part 1, Section 1.2, 1989.
[14] ASTM C1161-90, Standard test method for flexural strength of advanced ceramics at ambient temperature, Annual Book of ASTM Standards, vol. 15.01, ASTM, 1991, pp. 327–333.
[15] ASTM D790M-86, Standard test methods for flexural properties of unreinforced and reinforced plastics and electrical insulating materials, Annual book of ASTM Standards, vol. 08.01, ASTM, 1988, pp. 290–298.

[16] D.R. Larson, J.A. Coppola, D.P.H. Hasselman, Fracture toughness and spalling behaviour of high-Al_2O_3 refractories, J. Am. Ceram. Soc. 57 (1974) 417–421.
[17] ASTM E399-90, Standard test method for plane-strain fracture toughness of metallic materials, Annual Book of ASTM Standards, vol. 03.01, ASTM, 1991, pp. 485–515.
[18] ASTM D5045-91, Standard test methods for plane-strain fracture toughness and strain energy release rate of plastic materials, Annual Book of ASTM Standards, vol. 08.03, ASTM, 1991, pp. 728–736.
[19] W.F. Brown, J.E. Srawley, Plane strain crack toughness testing of high strength metallic materials, in: ASTM Special Technical Publication, No: 410, 1967.
[20] A.A. Griffith, The theory of rupture, in: Proceedings of the First International Congress for Applied Mechanics, 1924, pp. 55–63.
[21] R.W. Davidge, G. Tappin, The effective surface energy of brittle materials, J. Mater. Sci. 3 (1967) 165–173.
[22] R.W. Davidge, Mechanical Behaviour of Ceramics, Cambridge University Press, Cambridge, 1979.
[23] M.I. Mendelson, Average grain size in polycrystalline ceramics, J. Am. Ceram. Soc. 52 (1969) 443–446.
[24] D.P.H. Hasselman, Thermal stress resistance parameters for brittle refractory ceramics: a compendium, Am. Ceram. Soc. Bull. 49 (1970) 1033–1037.
[25] J.F. Shackelford, W. Alexander, J.S. Park (Eds.), CRC Materials Science and Engineering Handbook, CRC Press, Boca Raton, Florida, 1994.
[26] S.J. Burnett, Properties of Refractory Materials, UKAEA Research Group Report, Harwell, 1969.
[27] H. Hayaski, T. Saitou, N. Maruyama, H. Inaba, K. Kawamura, M. Mori, Thermal expansion coefficient of yttria stabilized zirconia for various yttria contents, Solid State Ionics 176 (2005) 613–619.
[28] C. Aksel, P.D. Warren, F.L. Riley, Fracture behaviour of magnesia and magnesia–spinel composites before and after thermal shock, J. Eur. Ceram. Soc. 24 (2004) 2407–2416.